

Elastic electron scattering form factors of deformed exotic Xe isotopesTongqi Liang,¹ Jian Liu,^{1,2,*} Zhongzhou Ren,³ Chang Xu,⁴ and Shuo Wang⁵¹*College of Science, China University of Petroleum (East China), Qingdao 266580, China*²*PCIF Key Laboratory of Oil and Gas Terahertz Spectroscopy and Photoelectric Detection, China University of Petroleum (East China), Qingdao 266580, China*³*School of Physics Science and Engineering, Tongji University, Shanghai 200092, China*⁴*Department of Physics, Nanjing University, Nanjing 210093, China*⁵*Shandong Provincial Key Laboratory of Optical Astronomy and Solar-Terrestrial Environment, Institute of Space Science, Shandong University, Weihai 264209, China*

(Received 13 May 2018; revised manuscript received 3 September 2018; published 10 October 2018)

Background: The positions of diffraction minima of Coulomb form factors $|F_C(q)|^2$ are important landmarks for electron scattering experiments, which are sensitive to the nuclear size. For the isotopic chain, previous studies show the minima of $|F_C(q)|^2$ have an outward shift as the target nucleus moves to the proton-rich side.

Purpose: Based on previous studies, the Coulomb form factors of Xe isotopes are further investigated by the deformed relativistic mean-field (RMF) model and distorted wave Born approximation (DWBA) method.

Method: First, the nuclear charge density distributions are calculated by the constrained calculations of deformed RMF model. Next, the axially deformed density distributions are expanded into multipole components. With the charge density multipoles, the Coulomb form factors of Xe isotopes are calculated by the DWBA method.

Results: For the nucleus with deformation, there are differences on the Coulomb form factors calculated from the spherical and deformed RMF models. For the Xe isotopic chain, the changing trend of $|F_C(q)|^2$ from the deformed RMF model is different from the results from the spherical RMF model at high momentum transfers.

Conclusions: The minima of $|F_C(q)|^2$ of isotopes are directly influenced by the nuclear deformation parameter β_2 , not just the charge radius R_C . For the studies of electron scattering, the nuclear deformation should be taken into account, especially in high momentum transfers.

DOI: [10.1103/PhysRevC.98.044310](https://doi.org/10.1103/PhysRevC.98.044310)**I. INTRODUCTION**

As an effective method of studying nuclear electromagnetic structure, elastic electron scattering is widely used in nuclear physics [1–6]. Compared with other methods, there is only electromagnetic force between electron and nuclei, which makes the method of electron scattering more clear and precise. In past decades, a large number of experimental results of stable nuclei have been obtained and analyzed under the assumption that nuclei are spherically symmetric [7]. In order to interpret the experimental scattering data, different theories of elastic electron scattering have been developed, including the plane-wave Born approximation (PWBA) [3,4], the eikonal approximation [8], and phase shift analysis method [9–11]. Among these methods, the eikonal approximation and phase shift analysis method are described as distorted-wave Born approximation (DWBA) because the nuclear Coulomb distortion effects are taken into account.

With the development of radioactive nuclear beam facilities [12], nuclear physicists began to study short-lived nuclei in 1980s. It became a popular issue because a lot of new properties were discovered on unstable nuclei [13–20], such as the neutron halo, the neutron skin, and the bubble nuclei.

The research of electron scattering on unstable nuclei is very valuable, which has aroused widespread attention. However, it is difficult to make targets from unstable nuclei. For this purpose, new-generation radioactive isotope (RI) beam facilities are built at RIKEN [19–21], and GSI [15,16]. With the new facilities, more exotic nuclei that is far from the β -stable line can be studied by electron scattering and the internal structure of unstable nuclei will be obtained.

To study the Coulomb form factors $|F_C(q)|^2$ of exotic nuclei theoretically, one valid scattering model is combining the mean-field model and DWBA method. With this scattering model, the $|F_C(q)|^2$ of many nuclei have been calculated to reflect their nuclear structure [22–28], such as the neutron halo and the proton halo of light nuclei. Although this method has achieved considerable success, there is still a problem that the target nuclei were mainly studied with spherical symmetry, and the effects of nuclear deformation were neglected. It has been confirmed experimentally and theoretically that most nuclei are deformed [29–32]. The influences of nuclear deformation on electron scattering are first discussed in Refs. [33,34]. In recent papers, the authors study the electron scattering off deformed nuclei by the deformed scattering model, which combines the deformed relativistic mean-field (RMF) model and DWBA method [35,36]. With this scattering model, the Coulomb form factors of deformed even-even nuclei and odd- A nuclei are investigated. Comparing with the Coulomb

*liujian@upc.edu.cn

form factors from the spherical scattering model, the results calculated by the deformed scattering model coincide with the experimental data better. Therefore, it is reasonable to investigate the nuclear structure by combining the deformed RMF model and DWBA method.

In this paper, we further extend the research of elastic electron scattering off deformed nuclei to the exotic nuclei. In a recent paper [21], the experimental Coulomb form factors of ^{132}Xe have been measured. It is the first electron scattering experiment performed successfully at the self-confining radioactive-isotope ion target (SCRIT) facility, which solves the problem of making targets from short-lived nuclei. Therefore, we choose xenon isotopes as the candidates to theoretically study the elastic electron scattering off exotic nuclei. In this paper, we first calculate the Coulomb form factors of ^{132}Xe from the spherical and deformed scattering models, and the results are compared with the new experimental data. Second, we discuss the changing trends of $|F_C(q)|^2$ of the Xe isotopic chain, which are calculated by the spherical and deformed scattering models, respectively. It can be seen that the changing trend of the diffraction minima of Coulomb form factors is not only related to the nuclear charge radii R_C but also to the nuclear deformation parameter β_2 . Finally, the constrained calculations of the RMF model are calculated to disentangle the effects of R_C and β_2 on $|F_C(q)|^2$. The relation between the nuclear deformation β_2 and the diffraction minima of $|F_C(q)|^2$ of Xe isotopic chains is discussed for the first time, which can be used as a useful guide for the coming experiments on the Xe exotic deformed nuclei.

This paper is divided into four parts: In Sec. II, the theoretical framework of deformed RMF model and DWBA method is provided. In Sec. III, the numerical results and discussions are presented. Finally, in Sec. IV, a summary is given.

II. THEORETICAL FRAMEWORK

In this section, the theoretical framework for studying the Coulomb form factors of deformed nuclei is presented. The starting point is the effective Lagrange density of the RMF model [37,38]:

$$\begin{aligned} \mathcal{L} = & \bar{\psi} \left\{ \gamma^\mu \left[i\partial_\mu - g_\omega \omega_\mu - \frac{g_\rho}{2} \rho_\mu^a \tau^a - \frac{e}{2} (1 + \tau^3) A_\mu \right] \right. \\ & - (M - g_s \sigma) \left. \right\} \psi \\ & + \frac{1}{2} \partial^\mu \sigma \partial_\mu \sigma - \frac{1}{2} m_\sigma^2 \sigma^2 - \frac{\kappa}{3!} (g_s \sigma)^3 - \frac{\lambda}{4!} (g_s \sigma)^4 \\ & - \frac{1}{4} \Omega^{\mu\nu} \Omega_{\mu\nu} + \frac{1}{2} m_\omega^2 \omega^\mu \omega_\mu + \frac{\xi}{4!} (g_\omega^2 \omega^\mu \omega_\mu)^2 \\ & - \frac{1}{4} \vec{R}^{\mu\nu} \cdot \vec{R}_{\mu\nu} + \frac{1}{2} m_\rho^2 \vec{\rho}^\mu \cdot \vec{\rho}_\mu \\ & - \frac{1}{4} F^{\mu\nu} F_{\mu\nu} + U_{\text{eff}}(\omega_\mu, \vec{\rho}^\mu), \end{aligned} \quad (1)$$

where the nonlinear ω - ρ coupling term is

$$U_{\text{eff}}(\omega_\mu, \vec{\rho}^\mu) = \Lambda_\nu (g_\rho^2 \vec{\rho}^\mu \vec{\rho}_\mu) (g_\omega^2 \omega^\mu \omega_\mu). \quad (2)$$

Applying the effective Lagrange density to the Euler-Lagrange equation, the motion equations of nucleons are

obtained. For axially deformed nuclei, the single-particle wave functions can be described by the series expansion of eigenfunctions of the axially deformed harmonic-oscillator potential in cylindrical coordinates. On the basis of the no-sea approximation and mean-field approximation, the Dirac equation of nucleons can be written as

$$[-i\boldsymbol{\alpha} \cdot \nabla + \beta[M - S(\mathbf{r})] + U(\mathbf{r})] \psi_i(\mathbf{r}) = \varepsilon_i \psi_i(\mathbf{r}), \quad (3)$$

where $S(\mathbf{r})$ is the scalar potential and $U(\mathbf{r})$ is the vector potential. Using the same method, the Klein-Gordon equations for mesons are obtained. After many iterative computations, the precise density distributions of proton and neutron can be obtained. Neglecting any effect from the charge distribution inside a finite-size neutron, the nuclear charge density can be derived by folding the point proton density with the single-proton charge distribution [39],

$$\rho_C(\mathbf{r}) = \int \rho_p(\mathbf{r}') \rho^p(|\mathbf{r} - \mathbf{r}'|) d\mathbf{r}', \quad (4)$$

where $\rho^p(r) = \frac{Q^3}{8\pi} e^{-Qr}$ with $Q = 842.61$ MeV.

The axially deformed charge density $\rho_C(r, z)$ can be expanded by the Legendre function [40]:

$$\begin{aligned} \rho_C(r, z) = & \sum_k \rho_k(R) P_k(\cos\theta) \\ = & \rho_0(R) + \rho_2(R) P_2(\cos\theta) + \dots, \end{aligned} \quad (5)$$

where the multipole components are

$$\rho_k(R) = \frac{2k+1}{2} \int_{-1}^1 P_k(\cos\theta) \rho(r, z) d(\cos\theta). \quad (6)$$

With the charge density multipoles, the Coulomb form factors can be investigated. The derivation of this formula is under the PWBA method, which is convenient for studying the effects of each density multipole on Coulomb form factors. In the PWBA method, the relationship between charge density and Coulomb form factors is

$$F_C(q) = \frac{1}{Z} \int \rho_C(\mathbf{r}) e^{i\mathbf{q}\cdot\mathbf{r}} d\mathbf{r}. \quad (7)$$

Squaring $F_C(q)$, the Coulomb form factors can be expanded into several Coulomb multipoles [34]:

$$|F_C(q)|^2 = \sum_{\lambda=0,2,\dots}^{2J} |F^{C\lambda}(q)|^2. \quad (8)$$

Owing to the elastic electron scattering, the initial and final angular momenta J of the ground states of target nuclei are the same. The Coulomb multipoles $F^{C\lambda}$ are related to the intrinsic multipole $\mathcal{F}^{C\lambda}$,

$$F^{C\lambda} = \langle Jk\lambda 0 | J\lambda Jk \rangle \mathcal{F}^{C\lambda}, \quad (9)$$

where the k represents the total spin projection along the nuclear symmetry axis. From this equation, the weights of intrinsic multipoles to Coulomb multipoles are given. For $\lambda = 0$, \mathcal{F}^{C0} is considered as the contributions of the spherical charge density distributions:

$$\mathcal{F}^{C0} = \frac{1}{Z} \int d^3r \rho_0(r) j_0(qr). \quad (10)$$

And for $\lambda \geq 2$, $\mathcal{F}^{C\lambda}$ represent the contributions of the deformed charge density multipoles:

$$\mathcal{F}^{C\lambda} = \frac{4\pi}{Z\sqrt{2\lambda+1}} \int r^2 \rho_\lambda(r) j_\lambda(qr) dr. \quad (11)$$

The results of PWBA method are not accurate because the distorted effects on the electron waves are not taken into account. In the following, we study the $C0$ multipole of Eq. (8) by solving the Dirac equation with the spherical Coulomb potential arising from $\rho_0(r)$:

$$[\boldsymbol{\alpha} \cdot \mathbf{p} + \beta m + V(r)]\Psi(\mathbf{r}) = E\Psi(\mathbf{r}). \quad (12)$$

The wave function $\Psi(\mathbf{r})$ can be expanded into the upper and lower spherical spinors with definite angular momentum. At large distances, the upper and lower spinors of the radial wave function is determined with the phase shift δ with orbital angular momentum l . By solving the Dirac equation (12), the spin-up δ_l^+ and spin-down δ_l^- can be calculated. With the phase shifts, the direct scattering amplitude and spin-flip scattering amplitude can be written as

$$f(\theta) = \frac{1}{2ik} \sum_{l=0}^{\infty} [(l+1)(e^{2i\delta_l^+} - 1) + (e^{2i\delta_l^-} - 1)] P_l(\cos\theta), \quad (13a)$$

$$g(\theta) = \frac{1}{2ik} \sum_{l=0}^{\infty} [e^{2i\delta_l^-} - e^{2i\delta_l^+}] P_l^1(\cos\theta), \quad (13b)$$

where P_l and P_l^1 are Legendre and associated Legendre functions, respectively. With the scattering amplitude, the $C0$ multipole can be obtained,

$$F^{C0}(q) = (|f(\theta)|^2 + |g(\theta)|^2) / \sigma_{\text{Mott}}, \quad (14)$$

where σ_{Mott} is the Mott scattering cross section.

For most nuclei, deformation is not very large, and the spherical multipole $C0$ is the main part of the $|F_C(q)|^2$. The higher multipoles $C\lambda$, which are several orders magnitude smaller than $C0$ multipole, can only influence the Coulomb form factors at the diffraction minima. Therefore, the $C0$ multipole is calculated by DWBA method and the higher multipoles $C\lambda$ are calculated by PWBA method. According to Eq. (8), for the elastic $0^+ \rightarrow 0^+$ scattering from even-even Xe isotopes, only the $C0$ multipole is contained in the $|F_C(q)|^2$.

III. NUMERICAL RESULTS AND DISCUSSION

With the formulas of Sec. II, the Coulomb form factors of Xe isotopes are investigated in this section, where the corresponding charge density distributions are calculated by the spherical and deformed RMF models, respectively. First, the theoretical $|F_C(q)|^2$ of ^{132}Xe from both the spherical and deformed scattering models are calculated and compared with the experimental data. Second, we investigate the changing trends of $|F_C(q)|^2$ for Xe isotopic chain from the deformed scattering model. Finally, the results from the constrained calculations are further discussed.

In Table I, we present the theoretical binding energies per nucleon B/A (MeV), charge root-mean-square (rms) radii R_C

TABLE I. Theoretical binding energies per nucleon B/A (MeV), charge rms radii R_C (fm), and deformation parameters β_2 calculated by the spherical and deformed RMF models with the NL3* parameter set. The experimental data are taken from Refs. [30,41,42].

	B/A(MeV)			R_C (fm)			β_2		
	Sphe.	Defo.	Expt.	Sphe.	Defo.	Expt.	Sphe.	Defo.	Expt.
^{126}Xe	8.33	8.42	8.44	4.75	4.78	4.77	0.00	0.20	0.19
^{128}Xe	8.34	8.43	8.44	4.76	4.78	4.78	0.00	0.19	0.18
^{130}Xe	8.35	8.43	8.44	4.77	4.79	4.78	0.00	0.16	0.17
^{132}Xe	8.36	8.42	8.43	4.78	4.79	4.79	0.00	0.12	0.14
^{134}Xe	8.36	8.41	8.41	4.79	4.80	4.79	0.00	0.08	0.12
^{136}Xe	8.36	8.40	8.40	4.80	4.80	4.80	0.00	-0.02	0.12
^{138}Xe	8.28	8.34	8.34	4.82	4.83	4.83	0.00	0.07	
^{140}Xe	8.21	8.28	8.29	4.84	4.86	4.86	0.00	0.14	0.11
^{142}Xe	8.14	8.22	8.23	4.87	4.88	4.88	0.00	0.18	

(fm), and deformation parameters β_2 of Xe isotopes, which are calculated by the spherical and deformed RMF models. The NL3* parameter set [43] is used during the calculations. The experimental data are also given for comparison. The charge rms radii R_C are calculated neglecting the effects of neutrons in this paper. Considering the corrections on R_C , the correction equation can be written as [44-46]

$$R_C^2 = R_p^2 + r_p^2 + \frac{N}{Z} r_n^2 + \frac{3}{4M^2} \langle r^2 \rangle_{\text{so}}, \quad (15)$$

where the first two terms represent the effects of the protons, which have already been considered from Eq. (4). The term $r_n^2 = -0.1161(22) \text{ fm}^2$ is the mean-square charge radius of the neutron. The third term $\frac{3}{4M^2} = 0.033 \text{ fm}^2$ is the Darwin-Foldy term. The $\langle r^2 \rangle_{\text{so}}$ represents the spin-orbit correction, which has tiny influences [46,47]. There are no obvious changes on R_C when the last three terms are taken into account in the calculation. Therefore, the charge rms radii R_C in this paper are calculated without corrections.

In Fig. 1, the B/A and R_C are plotted as functions of the mass number A . Combining the results in Table I and Fig. 1, it can be seen that for the B/A and R_C , the spherical and deformed results both agree with the experimental data, and the results from the deformed RMF model coincide with the experimental data better. The deformed R_C are larger than spherical one, which is due to the relation between the

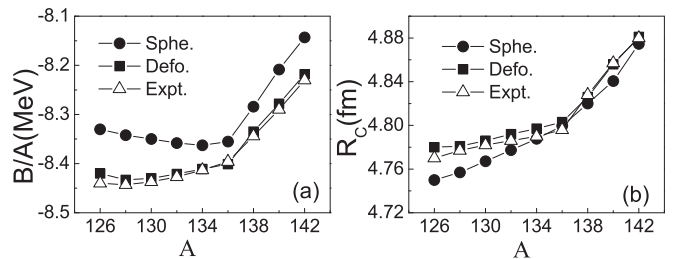


FIG. 1. Binding energies per nucleon B/A (MeV) and charge rms radii R_C (fm) for Xe isotopes calculated by the spherical and deformed RMF models with the NL3* parameter set. The experimental data are taken from Refs. [41,42].

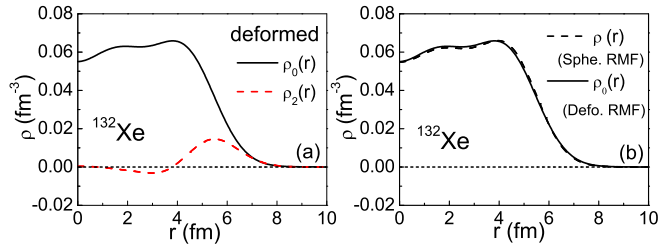


FIG. 2. (a) Charge density multipoles of ^{132}Xe from the deformed RMF model, which are calculated by Eqs. (5) and (6). (b) Comparison of spherical part $\rho_0(r)$ from the deformed RMF model with charge density distributions $\rho(r)$ from the spherical RMF model. The spherical and deformed RMF models are both calculated with the NL3* parameter set.

spherical and deformed radius [48]

$$R^2 = R_{\text{sph}}^2 \left(1 + \frac{5}{4\pi} \beta_2^2 \right). \quad (16)$$

The R_{sph} represents the spherical radius, which is proportional to $A^{1/3}$. Compared with the spherical radius R_{sph} , the deformed radius with $\beta_2 \neq 0$ is larger, which is same as the results in Table I. The experimental quadrupole deformations β_2 in Table I are extracted from $B(E2) \uparrow$ measurements, which are related to a stable quadrupole deformation in well-deformed nuclei. For $^{126-132}\text{Xe}$ in Table I, whose β_2 are larger than 0.12, these comparisons are acceptable. For $^{134-138}\text{Xe}$, which have small deformations, the comparisons of theoretical results with experimental data might be questionable. We further compare our results with other theoretical calculations, such as the finite-range droplet macroscopic model [29]. The results from the energy-deformation curves of RMF model coincide with other theoretical results. Therefore, the theoretical β_2 of $^{134-138}\text{Xe}$ in Table I with small deformations might be reliable. Combining Fig. 1 and Table I, it can be seen that the deformed RMF model can better describe the ground properties of Xe isotopes compared with the spherical RMF model.

The charge rms radii R_C in Table I can reflect nuclear ground properties of Xe isotopes, but it is not precise enough, because different charge distributions can correspond to the same R_C . However, the Coulomb form factor is unique for every charge distribution. Therefore, compared with R_C , the $|F_C(q)|^2$ can provide a more detailed description for the electromagnetic properties of nuclei. In the following, the Coulomb form factors of Xe isotopes are further studied by the DWBA method.

A. Coulomb form factors of ^{132}Xe

We first investigate the theoretical Coulomb form factors of ^{132}Xe from both the spherical and deformed scattering models, and compare them with the experimental data. By decomposing the charge density from the deformed RMF model with Eqs. (5) and (6), the multipole moment charge density distributions of ^{132}Xe are obtained and presented in Fig. 2(a), where the $\rho_0(r)$ and $\rho_2(r)$ represent the spherical distribution and quadrupole distribution, respectively. It can be seen that

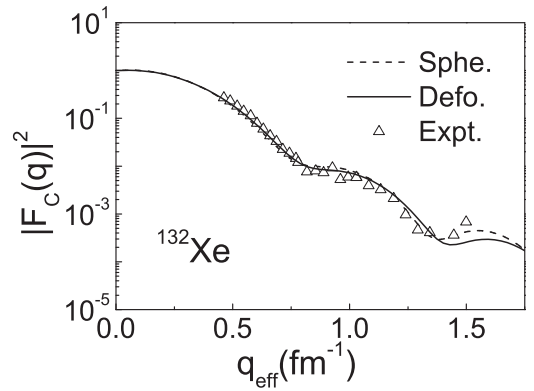


FIG. 3. Nuclear Coulomb form factors of ^{132}Xe calculated by DWBA method. The corresponding charge density distributions are obtained from the spherical and deformed RMF models with the NL3* parameter set. The experimental data are taken from Refs. [21].

for deformed charge density distributions, the values of the higher multipoles decrease rapidly with the multipole order k increasing. For $k > 2$, the multipole distributions ρ_k can be neglected. To compare the charge density distributions from the spherical and deformed RMF models, the spherical parts $\rho_0(r)$ from the deformed RMF model and $\rho(r)$ from the spherical RMF model are given in Fig. 2(b). There is a tiny difference between the spherical parts $\rho_0(r)$ and $\rho(r)$ in Fig. 2(b), which can be reflected in the Coulomb form factors at the higher momentum transfer region.

With the charge density distributions in Figs. 2(a) and 2(b), the Coulomb form factors $|F_C(q)|^2$ of ^{132}Xe are calculated and presented in Fig. 3. For comparison, the latest experimental data [21] are also given. In Fig. 3, it can be seen that the $|F_C(q)|^2$ from the spherical and deformed scattering models both agree with the experimental data well. At the higher momentum transfer region ($q > 1.25 \text{ fm}^{-1}$), the deformed and spherical $|F_C(q)|^2$ have a deviation. For the even-even nucleus ^{132}Xe , the $|F_C(q)|^2$ from the deformed scattering method only has $C0$ multipole with Eq. (8), which is related to the $\rho_0(r)$ in Fig. 2(a). In Fig. 2(b), there is a tiny difference between the $\rho_0(r)$ and $\rho(r)$, which results in the corresponding difference of $|F_C(q)|^2$ in Fig. 3.

B. Changing trends of $|F_C(q)|^2$ for the Xe isotopic chain

In this part, the changing trend of Coulomb form factors $|F_C(q)|^2$ of the Xe isotopic chain is systematically investigated with the deformed scattering method. The charge density distributions of ^{126}Xe , ^{128}Xe , and ^{130}Xe are calculated and presented in Fig. 4. The left three panels are charge density multipoles from the deformed RMF model. The right three panels are the comparisons of spherical parts $\rho_0(r)$ from the deformed RMF model with charge density distributions $\rho(r)$ from the spherical RMF model. Owing to the existence of $\rho_2(r)$, there are deviations between $\rho_0(r)$ and $\rho(r)$. The deviations can be reflected in the changing trend of $|F_C(q)|^2$ at the high momentum transfer region.

With the charge density distributions of the spherical RMF model in Fig. 4, we present the $|F_C(q)|^2$ of ^{126}Xe , ^{128}Xe , and

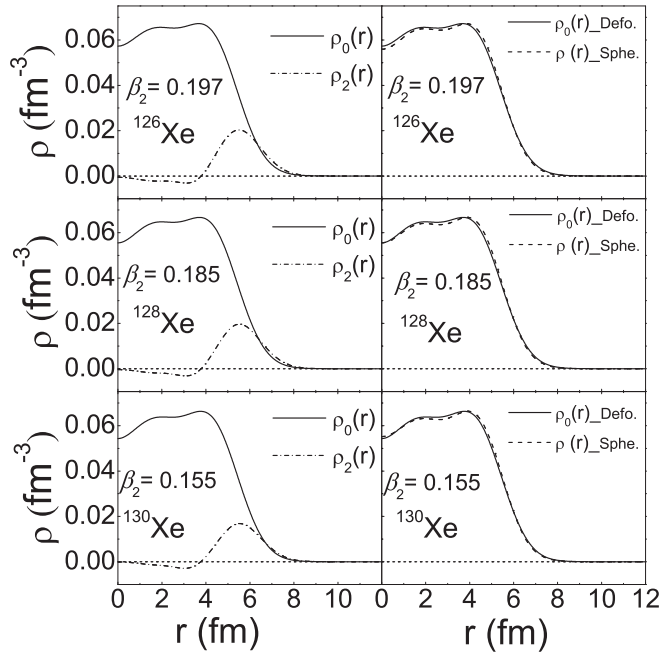


FIG. 4. Charge density distributions of even-even Xe isotopes ($A = 126, 128, 130$) from the spherical and deformed RMF models with NL3* parameter set. The left three panels are the charge density multipoles from the deformed RMF model. The right three panels are the comparisons of spherical parts $\rho_0(r)$ from the deformed RMF model with charge density distributions $\rho(r)$ from the spherical RMF model. The deformation parameters β_2 from the deformed RMF model are also given.

^{130}Xe from the spherical scattering method in Fig. 5, and the arrow shows the direction of the mass number A increasing. It can be seen that the $|F_C(q)|^2$ of ^{126}Xe , ^{128}Xe , and ^{130}Xe in Fig. 5 are close to each other. With the mass number A increasing, the diffraction minima of $|F_C(q)|^2$ have an inward shift, which is the same as the studies in previous papers [23–25].

In Fig. 6, we further present the $|F_C(q)|^2$ of ^{126}Xe , ^{128}Xe , and ^{130}Xe from the deformed scattering method. The corresponding R_C and β_2 are also given. The arrows show the directions of the mass number A and deformation parameter

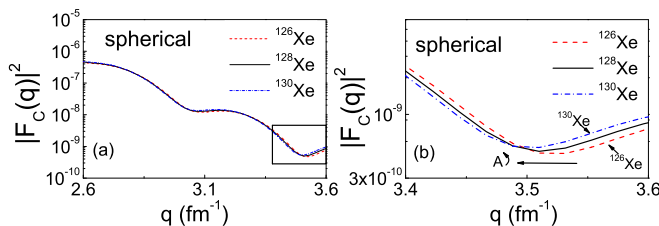


FIG. 5. The changing trend of Coulomb form factors of ^{126}Xe , ^{128}Xe , and ^{130}Xe , which are calculated by DWBA method. The corresponding charge density distributions are obtained from the spherical RMF model. The arrow shows the direction of the mass number A increasing. The range of the momentum transfer in panel (a) is $q = 2.6\text{--}3.6\text{ fm}^{-1}$. The range of the square frame ($q = 3.4\text{--}3.6\text{ fm}^{-1}$) in panel (a) is enlarged in panel (b).

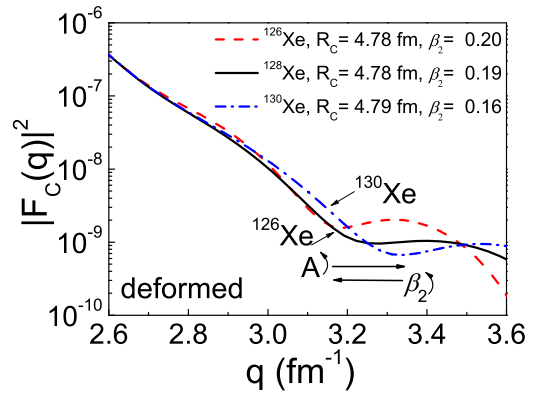


FIG. 6. The changing trend of Coulomb form factors of ^{126}Xe , ^{128}Xe , and ^{130}Xe , which are calculated by DWBA method. The corresponding charge density distributions are obtained from the deformed RMF model. The arrows show the directions of the mass number A and deformation parameter β_2 increasing.

β_2 increasing. Compared with the $|F_C(q)|^2$ from the spherical scattering method in Fig. 5, the diffraction minima of $|F_C(q)|^2$ of ^{126}Xe , ^{128}Xe , and ^{130}Xe from the deformed scattering method locate at different momentum transfers q , which is due to the nuclear deformation. Besides, in Fig. 6, with the mass number A increasing, the diffraction minima of $|F_C(q)|^2$ have an outward shift at the high momentum transfer region, which is opposite from the results from the spherical scattering method in Fig. 5. With the values of β_2 increasing, the diffraction minima of $|F_C(q)|^2$ have an inward shift in Fig. 6. The nuclear deformation has a significant influence on the changing trend of $|F_C(q)|^2$ of Xe isotopic chain. Therefore, the $|F_C(q)|^2$ are not only related to the charge radius R_C but also to the deformation parameter β_2 . This conclusion can be used to guide the coming experiments on elastic electron scattering off exotic nuclei.

For the electron scattering experiments of Xe isotopes in the SCRIT of RIKEN, it is said in Refs. [49,50] that the luminosity was estimated to be of order $10^{25}\text{ cm}^{-2}\text{ s}^{-1}$ for the present RI rate of 10^7 atoms s^{-1} , which is insufficient. However, the electron-beam power will be upgraded by increasing the electron gun current. The RI rate is increased to the order of 10^8 atoms s^{-1} for Xe isotopes, and the luminosity exceeds $10^{26}\text{ cm}^{-2}\text{ s}^{-1}$ [49,50]. Under these conditions, the electron scattering by Xe isotopes becomes feasible. However, the effects on $|F_C(q)|^2$ from the nuclear deformation in Fig. 6 mainly appear at high momentum transfers, which are small and difficult to be observed experimentally at present. If the electron scattering experiments at high momentum transfers are carried out in the future, the effects from deformation in Fig. 6 can be tested.

C. Disentangle the effects of R_C and β_2 on $|F_C(q)|^2$

From Figs. 5 and 6, one can see that the structure of the Coulomb form factor $|F_C(q)|^2$ is not only affected by the charge rms radius R_C , but also by the deformation parameter β_2 . In Fig. 6, the diffraction minima have an outward shift with the R_C increasing and β_2 decreasing. However, it is not clear

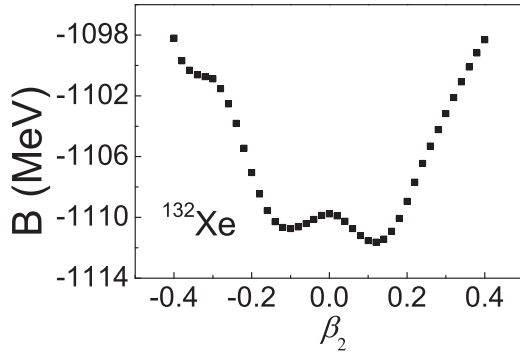


FIG. 7. Binding energies B of ^{132}Xe as a function of the deformation parameter β_2 from the constrained RMF calculations with NL3* parameter set.

what the dominant effect will be. They are quantities closely related and their combined effect is not easy to disentangle. To investigate the effects of R_C and β_2 on $|F_C(q)|^2$ conveniently, we use the PWBA method to calculate the diffraction minima of $|F_C(q)|^2$ of ^{132}Xe . The corresponding $\rho_C(\mathbf{r})$ of ^{132}Xe are computed by the constrained calculations of RMF model with the NL3* parameter set.

The binding energies B of ^{132}Xe from the constrained calculations of RMF model are plotted as a function of the deformation parameter β_2 in Fig. 7. The minimum of binding energy is located at $\beta_2 = 0.12$, where the binding energy per nucleon is same as the result in Table I. We choose the results constrained with $\beta_2 = 0.0$ and 0.4 to discuss the effects of R_C and β_2 on $|F_C(q)|^2$. The charge density multipoles of ^{132}Xe from the constrained calculations ($\beta_2 = 0.0$ and 0.4) are presented in Fig. 8. The corresponding $|F_C(q)|^2$ of ^{132}Xe calculated by PWBA method are also presented in Fig. 9.

With the constrained RMF calculations, we can study the relationship between β_2 and $|F_C(q)|^2$. In previous studies [45,51], the charge rms radius R_C and the first diffraction minimum of $|F_C(q)|^2$ are found to be inversely proportional. In Fig. 9, the diffraction minima of $|F_C(q)|^2$ with $\beta_2 = 0.0$ and 0.4 locate at the same positions in low momentum transfers. With the increase of q , the diffraction minima of $|F_C(q)|^2$ with $\beta_2 = 0.4$ have significant outward shifts at the high momentum transfer region; however, its R_C is larger than that with $\beta_2 = 0.0$. From Fig. 9, one can see that the nuclear deformation can also affect the nuclear Coulomb form factor

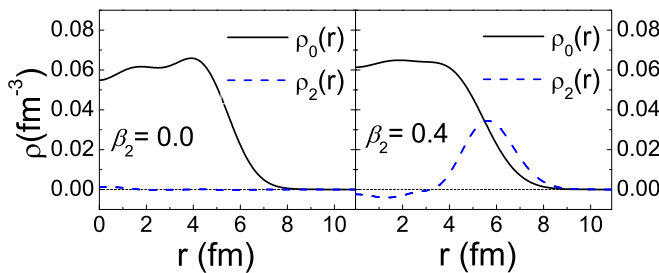


FIG. 8. Charge density multipoles of ^{132}Xe with $\beta_2 = 0.0$ and 0.4 from the constrained RMF calculations. The constrained RMF calculations are computed with the NL3* parameter set.

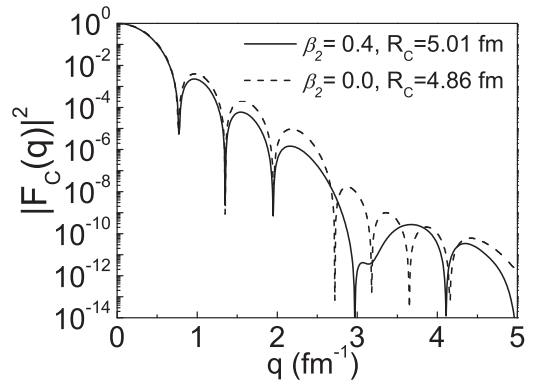


FIG. 9. The $|F_C(q)|^2$ of ^{132}Xe for $\beta_2 = 0.0$ and 0.4 calculated by PWBA method, where the corresponding $\rho_C(\mathbf{r})$ are obtained by the constrained RMF calculations with the NL3* parameter set.

$|F_C(q)|^2$. Therefore, the relationship between $|F_C(q)|^2$ and R_C needs to be further improved by taking into account the deformation parameter β_2 .

IV. SUMMARY

The elastic electron scattering of Xe isotopes are investigated systematically by the deformed scattering model in this paper. By combining the deformed RMF model and DWBA method, this paper aims to extend the research of elastic electron scattering off deformed nuclei to the region of exotic isotopes. For even-even Xe isotopes, there is only $C0$ multipole in their Coulomb form factors, which is related to the spherical part $\rho_0(r)$ from the deformed RMF model. The quadrupole distribution $\rho_2(r)$ leads to the difference between $\rho(r)$ from the spherical RMF model and $\rho_0(r)$. This difference can be reflected in the Coulomb form factors.

The investigations are divided into three parts. First, the theoretical Coulomb form factors $|F_C(q)|^2$ of ^{132}Xe are calculated and compared with the experimental data. The $|F_C(q)|^2$ from the spherical and deformed scattering model both coincide with the experimental data well. Second, we present the changing trends of $|F_C(q)|^2$ of ^{126}Xe , ^{128}Xe , and ^{130}Xe , where the corresponding charge density distributions are calculated by the spherical and deformed RMF models, respectively. With the mass number A increasing, the diffraction minima of $|F_C(q)|^2$ from the deformed scattering model have an outward shift at the high momentum transfer region, which are different from the results from the spherical scattering model. For studies of electron scattering, the nuclear deformation cannot be neglected, though its effects of deformation on $|F_C(q)|^2$ are not large and hard to be observed experimentally at present. Finally, we further disentangle the effects of R_C and β_2 on $|F_C(q)|^2$ with the constrained RMF calculations. For the same nucleus, the constrained RMF calculations with larger β_2 give the larger R_C ; however, the corresponding $|F_C(q)|^2$ have outward shifts at the high momentum transfer region. From the constrained RMF calculations with different β_2 , it is found that the $|F_C(q)|^2$ are not only related to the R_C but also to the β_2 . The studies of this paper can be served as a

useful guide for the coming experiments on electron scattering off the exotic deformed nuclei.

ACKNOWLEDGMENTS

The authors are grateful to Tiekuang Dong for valuable discussions and careful reading of the manuscript. This work

is supported by the National Natural Science Foundation of China (Grants No. 11505292, No. 11535004, No. 11575082, No. 11761161001, and No. 11605105), by the Shandong Provincial Natural Science Foundation, China (Grant No. BS2014SF007), by the Fundamental Research Funds for the Central Universities (Grant No. 17CX02044), and by International S&T Cooperation Program of China (Grant No. 2016YFE0129300).

- [1] I. Sick and D. Trautmann, *Phys. Rev. C* **89**, 012201 (2014).
- [2] R. Hofstadter, *Rev. Mod. Phys.* **28**, 214 (1956).
- [3] R. S. Willey, *Nucl. Phys.* **40**, 529 (1963).
- [4] T. de Forest and J. D. Walecka, *Adv. Phys.* **15**, 1 (1966).
- [5] H. Überall, *Electron Scattering from Complex Nuclei* (Academic Press, New York, 1971).
- [6] J. D. Walecka, *Electron Scattering for Nuclear and Nucleon Structure* (Cambridge University Press, Cambridge, UK, 2001).
- [7] H. De Vries, C. W. De Jager, and C. De Vries, *At. Data Nucl. Data Tables* **36**, 495 (1987).
- [8] A. Baker, *Phys. Rev.* **134**, B240 (1964).
- [9] D. Yennie, F. Boos, and D. Ravenhall, *Phys. Rev.* **137**, B882 (1965).
- [10] J. Heisenberg, in *Advances in Nuclear Physics*, Advances in the Physics of Particles and Nuclei, edited by J. W. Negele *et al.*, Vol. 12 (Springer, Boston, MA, 1981), Chap. 2, pp. 61–133.
- [11] M. Nishimura, E. M. de Guerra, and D. W. L. Sprung, *Nucl. Phys. A* **435**, 523 (1985).
- [12] I. Tanihata, *Prog. Part. Nucl. Phys.* **35**, 505 (1995).
- [13] E. Garrido and E. M. de Guerra, *Nucl. Phys. A* **650**, 387 (1999).
- [14] E. M. de Guerra, E. Garrido, and P. Sarriguren, Challenges in nuclear structure, in *Proceedings of the 7th International Spring Seminar on Nuclear Physics* (World Scientific, Singapore, 2002).
- [15] H. Simon, *Nucl. Phys. A* **787**, 102 (2007).
- [16] A. N. Antonov, M. K. Gaidarov, M. V. Ivanov, D. N. Kadrev, M. Aïche, G. Barreau, S. Czajkowski, B. Jurado, G. Belier, A. Chatillon *et al.*, *Nucl. Instrum. Methods Phys. Res. Sect. A* **637**, 60 (2011).
- [17] T. Suda, *J. Phys.: Conf. Ser.* **267**, 012008 (2011).
- [18] T. Suda and M. Wakasugi, *Prog. Part. Nucl. Phys.* **55**, 417 (2005).
- [19] M. Wakasugi, T. Emoto, Y. Furukawa, K. Ishii, S. Ito, T. Koseki, K. Kurita, A. Kuwajima, T. Masuda, A. Morikawa *et al.*, *Phys. Rev. Lett.* **100**, 164801 (2008).
- [20] T. Suda, M. Wakasugi, T. Emoto, K. Ishii, S. Ito, K. Kurita, A. Kuwajima, A. Noda, T. Shirai, T. Tamae *et al.*, *Phys. Rev. Lett.* **102**, 102501 (2009).
- [21] K. Tsukada, A. Enokizono, T. Ohnishi, K. Adachi, T. Fujita, M. Hara, M. Hori, T. Hori, S. Ichikawa, K. Kurita *et al.*, *Phys. Rev. Lett.* **118**, 262501 (2017).
- [22] Z. Wang and Z. Ren, *Phys. Rev. C* **70**, 034303 (2004).
- [23] A. N. Antonov, D. N. Kadrev, M. K. Gaidarov, E. M. Moya de Guerra, P. Sarriguren, J. M. Udias, V. K. Lukyanov, E. V. Zemlyanaya, and G. Z. Krumova, *Phys. Rev. C* **72**, 044307 (2005).
- [24] X. Roca-Maza, M. Centelles, F. Salvat, and X. Viñas, *Phys. Rev. C* **78**, 044332 (2008).
- [25] X. Roca-Maza, M. Centelles, F. Salvat, and X. Viñas, *Phys. Rev. C* **87**, 014304 (2013).
- [26] S. Karataglidis and K. Amos, *Phys. Lett. B* **650**, 148 (2007).
- [27] J. Liu, X. Zhang, C. Xu, and Z. Ren, *Nucl. Phys. A* **948**, 46 (2016).
- [28] K. S. Jassim, A. A. Al-Sammarae, F. I. Sharrad, and H. A. Kassim, *Phys. Rev. C* **89**, 014304 (2014).
- [29] P. Möller, J. R. Nix, W. D. Myers, and W. J. Swiatecki, *At. Data Nucl. Data Tables* **59**, 185 (1995).
- [30] S. Raman, C. W. Nestor, and P. Tikkanen, *At. Data Nucl. Data Tables* **78**, 1 (2001).
- [31] N. J. Stone, *At. Data Nucl. Data Tables* **90**, 75 (2005).
- [32] G. Scamps, D. Lacroix, G. G. Adamian, and N. V. Antonenko, *Phys. Rev. C* **88**, 064327 (2013).
- [33] E. M. de Guerra, *Ann. Phys. (N.Y.)* **128**, 286 (1980).
- [34] E. M. de Guerra, *Phys. Rep.* **138**, 293 (1986).
- [35] J. Liu, C. Xu, and Z. Ren, *Phys. Rev. C* **95**, 044318 (2017).
- [36] J. Liu, C. Xu, S. Wang, and Z. Ren, *Phys. Rev. C* **96**, 034314 (2017).
- [37] B. G. Todd-Rutel and J. Piekarewicz, *Phys. Rev. Lett.* **95**, 122501 (2005).
- [38] R. Utama, W.-C. Chen, and J. Piekarewicz, *J. Phys. G* **43**, 114002 (2016).
- [39] W. Greiner and J. Reinhardt, *Quantum Electrodynamics* (Springer-Verlag, Berlin, 1992).
- [40] E. M. de Guerra, P. Sarriguren, and J. A. Caballero, *Nucl. Phys. A* **529**, 68 (1991).
- [41] M. Wang, G. Audi, F. G. Kondev, W. J. Huang, S. Naimi, and X. Xu, *Chin. Phys. C* **41**, 030003 (2017).
- [42] I. Angeli and K. P. Marinova, *At. Data Nucl. Data Tables* **99**, 69 (2013).
- [43] G. A. Lalazissis, S. Karatzikos, R. Fossion, D. P. Arteaga, A. V. Afanasjev, and P. Ring, *Phys. Lett. B* **671**, 36 (2009).
- [44] A. Ong, J. C. Berengut, and V. V. Flambaum, *Phys. Rev. C* **82**, 014320 (2010).
- [45] P. Sarriguren, M. K. Gaidarov, E. M. de Guerra, and A. N. Antonov, *Phys. Rev. C* **76**, 044322 (2007).
- [46] C. J. Horowitz and J. Piekarewicz, *Phys. Rev. C* **86**, 045503 (2012).
- [47] J. Liu, Z. Ren, C. Xu, and R. Xu, *Phys. Rev. C* **88**, 054321 (2013).
- [48] B. Cheal and K. T. Flanagan, *J. Phys. G* **37**, 113101 (2010).
- [49] T. Ohnishi, S. Ichikawa, K. Koizumi, K. Kurita, Y. Miyashita, R. Ogawara, S. Tamaki, M. Togasaki, and M. Wakasugi, *Nucl. Instrum. Methods Phys. Res. Sect. B* **317**, 357 (2013).
- [50] T. Ohnishi, M. Hara, T. Hori, S. Ichikawa, M. Watanabe, M. Wakasugi, K. Adachi, A. Enokizono, T. Fujita, M. Hori *et al.*, PoS (INPC2016) 088 (2016).
- [51] D. W. L. Sprung, N. Yamanishi, and D. C. Zheng, *Nucl. Phys. A* **550**, 89 (1992).